Band structure parameters of wurtzite and zinc-blende GaAs under strain in the GW approximation

Tawinan Cheiwchanchamnangij and Walter R. L. Lambrecht
Department of Physics, Case Western Reserve University, Cleveland, Ohio 44106-7079, USA
(Received 19 April 2011; published 26 July 2011)

Quasiparticle self-consistent GW calculations are used to study the band structure in wurtzite and zinc-blende GaAs. The band-gap change between wurtzite and zinc blende is found to be sensitive to lattice constant and k-point convergence of the GW self-energy. Furthermore, the conduction-band minimum can switch between Γ_1 and Γ_3 character as a function of strain and the valence-band maximum can cross over from Γ_5 to Γ_1 under compressive uniaxial strain. The Kohn-Luttinger and Rashba-Sheka-Pikus effective Hamiltonian band structure parameters of zinc-blende and wurtzite GaAs, respectively, are determined from these first-principles band structure calculations. The uniaxial and homogeneous strain dependence of the band structure are studied and summarized in the appropriate strain deformation potential parameters.

DOI: 10.1103/PhysRevB.84.035203 PACS number(s): 71.20.Mq, 71.15.Mb, 71.70.Fk

I. INTRODUCTION

Recently, it has become possible to grow high-quality nanowires of semiconductors with mixed zinc-blende and wurtzite structure[1–4] for III-V semiconductors, which normally only exhibit the zinc-blende (ZB) structure in bulk form. In order to model the electronic and optical properties within an envelope approximation, one needs to know the band structure parameters of the wurtzite (WZ) structure for these materials. These nanowires may occur in different strain states and, thus, it is also important to study the strain dependence of the band structure. In this paper, we use first-principles calculations to study the strain dependence of the band structure of wurtzite GaAs. We compare our calculations to previous theoretical studies.[4–6]

II. METHOD

The calculations are performed using the full-potential linearized muffin-tin orbital method[7] (FP-LMTO). The equilibrium structural parameters are determined within density functional theory in the local density approximation[8,9] (LDA). The von Barth–Hedin exchange correlation functional is used.[10] In order to obtain accurate band structures, we use the quasiparticle self-consistent GW method (QSGW).[11–13]

We note that LDA might not be sufficient to extract accurate band splittings such as the crystal field splitting. In fact, the threefold-degenerate valence band of ZB splits into a Γ_5 and Γ_1 state in WZ, which correspond, respectively, to in-plane X,Y-like and perpendicular to the plane Z-like states. The conduction-band minimum is Γ_1 and is by symmetry allowed to interact with the Γ_1 crystal field split-off state. Thus, an underestimate of the gap (by LDA) is expected to lead to an overestimate of the crystal field splitting.

As is well known,[14] the GW approximation (GWA) is the first term in an expansion of the self-energy of one-particle excitations in the screened Coulomb interaction W. While usually it is applied as a one-shot correction to LDA, assuming LDA wave function to calculate both the one-electron Green's function and the dynamically screened Coulomb interaction, in QSGW, one obtains a new nonlocal (but energy-independent) exchange-correlation potential from the self-energy Σ,

$$V_{xc}^{\mathrm{QSGW}} = \frac{1}{2}\sum_{nm} |\Psi_n\rangle \Re[\Sigma_{nm}(E_n) + \Sigma_{nm}(E_m)]\langle\Psi_m|, \quad (1)$$

from which a new GW calculation is performed. When this procedure is iterated to convergence, the Kohn-Sham eigenvalues of the above exchange-correlation potential become equal to the GW quasiparticle energies. This procedure, combined with an accurate and efficient scheme for calculation of the GW self-energy based on the FP-LMTO band structure method, and a mixed basis set for expanding all two-electron operators, has been shown to give very accurate results for a wide variety of systems. For most semiconductors, it slightly but systematically overestimates the band gaps because of the underscreening of the random-phase approximation used in the GWA. The mixed basis set combines products of muffin-tin orbitals with additional plane waves to span the interstitial region. Details can be found in Refs. 12 and 13. It is found that a slight scaling of the self-energy Σ_{xc} by a factor 0.8 provides band gaps in agreement with experiment to better than 0.1 eV.

A unique feature of the above QSGW scheme is that the above exchange-correlation potential can be expanded in a basis of muffin-tin orbitals in real space. This then allows us to perform the GW calculations on a relatively sparse k mesh, Fourier transforming to real space and back to an arbitrary fine k mesh or to the k points of interest for the bands along symmetry lines. This procedure is important to obtain accurate effective masses and related parameters, which is the main goal of this paper.

The calculations are performed first in the scalar relativistic approximation and spin-orbit coupling is then added by rediagonalizing the double-sized Hamiltonian matrices with the above V_{xc}^{QSGW} and spin-orbit coupling calculated form the corresponding potentials within the spheres. Spin-orbit coupling arises mostly from the inner parts of the atom, so this is a good approximation.

In the LDA self-consistent calculation, we used a $10 \times 10 \times 10$ k-point mesh, which resulted in 150 irreducible k points after symmetry operations are applied. Moreover, $32 \times 32 \times 55$ divisions are used to specify the uniform mesh density along the x, y, and z directions in direct space for

the smooth parts of the potential, charge density, and wave functions. A double κ-basis set was used as envelope functions up to f states in the first κ and up to d states in second κ. Semicore Ga-3d bands were included as local orbitals.[15,16] The calculations were converged to within a change in total energy less than 10^{-6} Ry.

Starting from the above LDA band structures, the QSGW calculation is performed with a $4 \times 4 \times 4$ k-point mesh for WZ. Four floating orbitals (orbitals centered on interstitial sites) are added to improve the basis set even further for high-energy unoccupied states. The latter are not augmented, so they have only an envelope function but no augmentation sphere.

On the other hand, the GW self-energy is very sensitive to convergence of the basis set and k points. Our present calculation differs slightly from that in Ref. 13. We treated Ga-4d states as band and Ga-3d states as "local orbitals," while Kotani *et al.*[13] treated Ga-3d as bands and Ga-4d as localized orbitals and also included high-lying As-5s as local orbitals, which we omit. While their calculation is better converged with respect to basis set, it overestimates the gap by about 0.2 eV, as usual. We found that, with our basis set, the gap for ZB GaAs is very close to the experimental value and no *a posteriori* scaling by 0.8 is required. For the present purpose, all we care about is good agreement with experiment for ZB and equivalent level of convergence for WZ, not studying the absolute convergence of the GWA itself.

In order to accurately obtain the band-gap difference between ZB and WZ, we found again that the k-point convergence is crucial. To obtain maximal systematic error cancellation, it is important to use an exactly equivalent k-point convergence of the GW self-energy. This can be achieved by treating the ZB as a three- (111-) layer cell and WZ as a two- (0001-) layer cell and using a $4 \times 4 \times 2$ mesh for ZB and $4 \times 4 \times 3$ mesh for WZ.

The valence-band manifold near the valence-band maximum are fit to the Rashba-Sheka-Pikus Hamiltonian, which is described in Bir and Pikus[17], given by

$$\begin{aligned}\hat{H} = {} & \Delta_1 L_z^2 + \Delta_2 L_z \sigma_z + \sqrt{2}\Delta_3 (L_+ \sigma_- + L_- \sigma_+) \\ & + \left(A_1 + A_3 L_z^2\right) k_z^2 + \left(A_2 + A_4 L_x^2\right)\left(k_x^2 + k_y^2\right) \\ & - A_5 (L_+^2 k_-^2 + L_-^2 k_+^2) \\ & - 2i A_6 k_z ([L_z, L_+] k_- - [L_z, L_-] k_+) \\ & + A_7 (k_- L_+ + k_+ L_-), \end{aligned} \tag{2}$$

where $L_\pm = \pm(i/\sqrt{2})(L_x \pm i L_y)$, $\sigma_\pm = \pm(i/\sqrt{2})(\sigma_x \pm i\sigma_y)$, and $k_\pm = k_x \pm i k_y$. In this equation, Δ_1 is the crystal field splitting, while Δ_2 and Δ_3 represent spin-orbit coupling parameters required by hexagonal symmetry. The inverse mass parameters (A_i, for $i = 1,2,3,4$) for in-plane and along z directions are obtained by fitting parabolic curves to the first-principles bands without spin-orbit coupling. The remaining parameters are estimated from the quasicubic approximation and the A_7 parameter is obtained by fitting the behavior near the avoided band crossing of the light hole and crystal field split-off band. The procedure is similar to that followed in Kim e*t al.*[18] The spin-orbit parameters are obtained from the splittings at Γ in the first-principles calculation and then combined with the above mass parameters to diagonalize the full 6×6 Hamiltonian and compared to the directly calculated bands with spin-orbit splitting. The k range over which the parabolic fits is made is such that the bands of the model and the first-principles calculation agree within an energy range of about 200 meV.

III. RESULTS

A. Structure

First, we consider the equilibrium structural properties. The equilibrium volume per GaAs pair V^w (i.e., half the volume of the wurtzite primitive cell) lattice constant a, c/a ratio and internal parameter u as well as the zinc-blende lattice constant a^z and volume V^z are given in Table I for both LDA and generalized gradient approximation (GGA). The experimental value included in the table is for zinc-blende GaAs. Our calculations give the volume of zinc-blende GaAs in LDA to be 44.23 Å^3 and 47.45 Å^3 in GGA, in both cases very close to that of wurzite, to within 0.1 %.

The u parameter is found to behave linearly with c/a according to the equation

$$u(\eta) = u(\eta_0) + \xi(\eta - \eta_0) \tag{3}$$

with a slope parameter $\xi = -0.089$, where η is c/a ratio and η_0 is c/a ratio at the equilibrium. This linear relation results from the internal strain parameter in the system.[19]

B. Band gaps

First, let us check the accuracy of our QSGW approach for ZB GaAs. At the experimental lattice constant, we find the QSGW gap with our present basis set to be 1.595 eV without spin-orbit correction. By including the spin-orbit coupling, we find 1.503 eV. The gap reduction by the spin-orbit coupling amounts to about 1/3 of the spin-orbit splitting for which we find 0.32 eV, very close to the experimental value of 0.341 eV.[20] The experimental band gap is 1.519 eV.[20] Thus, we have excellent agreement to within 16 meV without making any further corrections to the GW self-energy.

As is well known, LDA or GGA significantly underestimate the band gap. In the present case, for ZB GaAs at the LDA lattice constant we obtain 0.320 eV. But, usually one assumes that one can nevertheless obtain band-gap differences between two structures such as ZB and WZ rather accurately because the systematic LDA error is assumed to be similar for both structures. However, LDA or GGA also influences the lattice constant and this, in turn, has an effect on the band gap. We calculated the band gaps at the LDA, GGA, and experimental lattice volume all using the QSGW approach. As mentioned in Sec. II, to ensure exactly equal k-point convergence between ZB and WZ in the GW self-energy, we used a three-layer ZB

TABLE I. Structural parameters of wurtzite and zinc-blende GaAs.

	Zinc blende		Wurtzite			
	a^z (Å)	V^z (Å^3)	V^w (Å^3)	a (Å)	c/a	u
LDA	5.614	44.23	44.20	3.955	1.650	0.3735
GGA	5.746	47.45	47.44	4.050	1.649	0.3741
Experiment	5.653	45.17				

TABLE II. QSGW band gaps (in eV) between high-symmetry points in zinc-blende and wurtzite GaAs at three lattice constants.

	Zinc blende		Wurtzite	
	$\Gamma_{15v}-\Gamma_{1c}$	$\Gamma_{15v}-L_{1c}$	$\Gamma_{5v}-\Gamma_{1c}$	$\Gamma_{5v}-\Gamma_{3c}$
a_{LDA}	1.774	1.959	1.861	1.712
a_{GGA}	1.189	1.703	1.284	1.497
a_{expt}	1.595	1.884	1.675	1.646

cell and a two-layer WZ cell with 2/3 of the number of k points along the c direction in ZB than in WZ.

We found that an additional complication arises in understanding the trend of the minimum gap: the conduction-band minimum (CBM) in WZ GaAs changes symmetry character as function of lattice constant. In Table II, we give the QSGW gaps (without spin-orbit coupling) for WZ and ZB for specific conduction-band states. For the GGA lattice constant (larger than the experimental one), the CBM in WZ is Γ_{1c} as expected, but for the experimental lattice constant and the LDA lattice constant (volume compression), the Γ_{3c} state becomes the conduction band. The latter is closely related to the ZB lowest conduction band at L, which is folded on to Γ by the doubling of the cell in the c direction.

As can be seen in Fig. 1, the ZB $\Gamma_{15v}-L_{1c}$ and WZ $\Gamma_{5v}-\Gamma_{3c}$ gaps are nearly parallel as a function of volume change, showing that they have the same deformation potential. The same is true for the ZB $\Gamma_{15v}-\Gamma_{1c}$ and WZ $\Gamma_{5v}-\Gamma_{1c}$ gaps. There is a *downward* shift from the indirect $\Gamma_{15v}-L_{1c}$ gap in ZB to the pseudodirect $\Gamma_{5v}-\Gamma_{3c}$ gap in WZ, but a slight *upward* shift of the direct gap from ZB to WZ. The latter is consistent with the usual trend in other materials where ZB-WZ polytypism has been observed, e.g., GaN, AlN.

As a result, the minimum gap in WZ changes from being Γ_{1c}-like for the GGA lattice constant to becoming Γ_{3c}-like at the LDA lattice constant, and the crossover occurs very close to the experimental lattice constant. In ZB, the conduction-band minimum stays at Γ_{1c}.

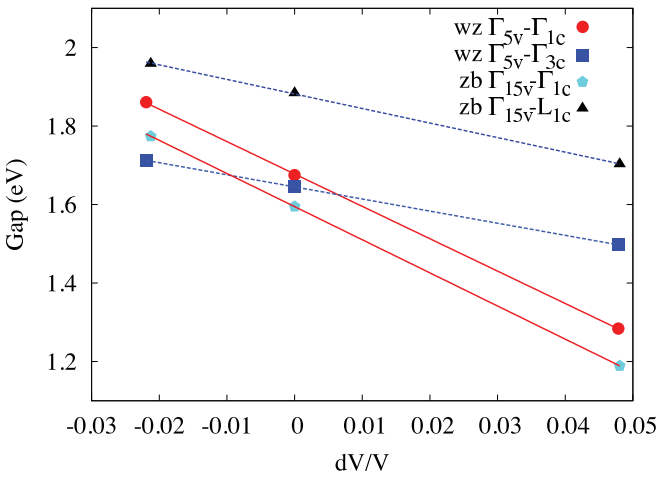

FIG. 1. (Color online) $\Gamma_{5v}-\Gamma_{1c}$ (circle) and $\Gamma_{5v}-\Gamma_{3c}$ (square) gaps of wurtzite structure and $\Gamma_{15v}-\Gamma_{1c}$ (pentagon) and $\Gamma_{15v}-L_{1c}$ (triangle) gaps of zinc-blende structure as a function of change in volume dV/V relative to the experimental volume.

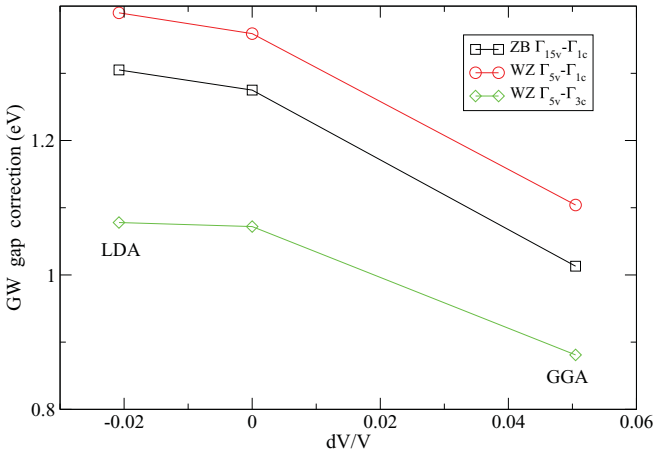

FIG. 2. (Color online) GW correction to the band gap as function of lattice constant and for different conduction-band states.

We now turn to the LDA or GGA to GW gap correction. Figure 2 shows the gap corrections at the three lattice constants for the different types of gaps. We can see that the gap correction is slightly larger by about 0.1 eV for the WZ than for the ZB corresponding direct gaps at Γ for each lattice constant. The gap correction also slightly decreases with increasing lattice constant. We should note that, at the GGA lattice constant, we compare GW with GGA rather than with LDA. Thus, the GW-GGA gap correction seems to be a bit smaller than for LDA, but all gap corrections vary only in a narrow range between 1.0 and 1.4 eV. So, to this precision, one can indeed use LDA or GGA to obtain gap changes, but in this case, the gap change is actually smaller than this and thus we conclude that GGA or LDA are insufficient to obtain such small gap differences between two structures. Furthermore, the GW correction for the Γ_{3c} state is significantly smaller than for the Γ_{1c} state. In other words, the Γ_{3c} gap is lowered relative to the Γ_{1c} in GW. GW does not lead to a uniform scissor shift as is often approximately assumed.

We believe that the controversial results about the gap change from ZB to WZ in the previous literature stems in part from this change in the conduction-band character in wurtzite, in part on the sensitivity to lattice constant used, and in part on the sensitivity of the GW self-energy to k-point convergence.

The slopes of the various band gaps versus volume change dV/V define the corresponding hydrostatic deformation potentials $dE_g^i/d\ln V = a^i$ for each type of gap i and are given in Table III.

TABLE III. Band-gap deformation potentials.

Gap type	$a^i = dE_g^i/d\ln V$ (eV)
ZB $\Gamma_{15v}-\Gamma_{1c}$	−8.44
ZB $\Gamma_{15v}-L_{1c}$	−3.71
WZ $\Gamma_{5v}-\Gamma_{1c}$	−8.25
WZ $\Gamma_{5v}-\Gamma_{3c}$	−3.09

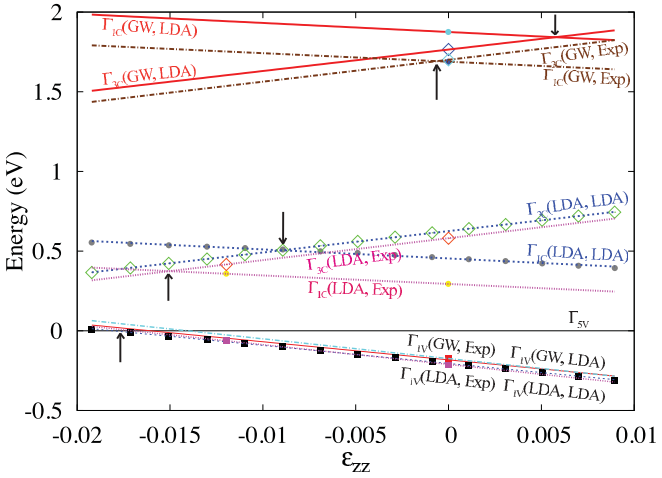

FIG. 3. (Color online) Energy level differences of the Γ_{1v}, Γ_{1c}, and Γ_{3c} states relative to the Γ_{5v} as a function of uniaxial strain ϵ_{zz} in wurtzite GaAs. The first label with each line gives the method used (LDA or GW) and the second label gives the lattice constant at which the calculation is performed (LDA or experiment).

C. Uniaxial-strain-induced band crossings

Next, we examine the valence-band and conduction-band behavior in wurtzite as a function of uniaxial strain along the c axis. In Fig. 3, we can see that at zero strain, the Γ_{5v} level (X,Y-like states) lie above the Γ_{1v} level, with a positive crystal field splitting $\Delta_1 = 212$ meV for the LDA calculation and $\Delta_1 = 186$ meV for the QSGW calculation. We first focus on the lines labeled LDA lattice constant. As mentioned earlier, as the gap increases, the crystal field splitting decreases slightly. However, under compressive strain, the crystal field splitting decreases and, at a strain of $\epsilon_{zz} = -1.5 \times 10^{-2}$ for the LDA calculation and $\epsilon_{zz} = -1.8 \times 10^{-2}$ for the QSGW calculation, the levels cross.

We also find a crossing of the conduction bands between the Γ_{1c} and Γ_{3c} bands. As already mentioned, the latter can be viewed as a folded L state of the zinc-blende structure. The $\Gamma_{3c} - \Gamma_{1c}$ crossing is thus related to a direct-to-indirect gap transition in zinc-blende GaAs. We found indeed that under uniaxial strain along the [111] direction, the CBM switches from Γ to the L point at a strain of $e_{[111]} = -0.08$. Recently, such a transition was observed under shock-wave high-pressure experiments.[21]

We note that the corresponding lines are almost exactly parallel in GW and LDA, thus, the strain dependence is already well described by LDA. Our LDA calculation suggests that the conduction bands will cross at a compressive strain $\epsilon_{zz} = -9.0 \times 10^{-3}$, but QSGW predicts the crossing to occur already for a tensile strain $\epsilon_{zz} = 2.7 \times 10^{-3}$. Therefore, for LDA, the minimum band gap changes from $\Gamma_{5v} - \Gamma_{1c}$ to $\Gamma_{5v} - \Gamma_{3c}$ character after the conduction-band crossing. Then, it changes from $\Gamma_{5v} - \Gamma_{3c}$ to $\Gamma_{1v} - \Gamma_{3c}$ after the valence-band crossing.

This should have important effects on the optical properties, since the $\Gamma_{5v} - \Gamma_{1c}$ transition is dipole allowed for polarization perpendicular to the c axis ($\mathbf{E} \perp c$), while the $\Gamma_{1v} - \Gamma_{1c}$ transition is dipole allowed for polarization parallel to the c axis ($\mathbf{E} \parallel c$). On the other hand, the transitions from Γ_{5v} and Γ_{1v} to Γ_{3c} are both dipole forbidden. While in absorption, it is possible to observe the transitions to the Γ_{1c} state even if it is not the lowest conduction-band state, luminescence at low temperature would be strongly suppressed with a Γ_{3c} conduction-band minimum because the higher level would not be populated at low temperature. So, LDA predicts that we would start out with a dipole-allowed transition polarized in the plane in luminescence, but we would never observe a strong polarization parallel to the c axis under compressive strain because the conduction bands already have switched before the valence bands switch. The QSGW calculations predict that already at zero strain, the conduction bands have switched to a Γ_{3c} minimum and, hence, luminescence would be suppressed in wurtzite even for the in-plane polarization. One would need to go to a slight tensile strain to obtain a strong dipole-allowed transition.

To test these predictions further, we must again consider how sensitive the results are to the exchange-correlation potential used in determining the structure. As is well known, LDA underestimates the equilibrium volume, while the generalized gradient approximation slightly overestimates it. The strain equal zero point therefore depends on whether we use LDA or GGA. We thus also performed QSGW calculations starting from the GGA lattice constants and at a lattice volume corresponding to the experimental volume of zinc blende but with the same c/a and u as before. In fact, we find that GGA and LDA give almost the same c/a ratio and u as shown before, so the only relevant parameter is the volume per GaAs pair.

We therefore think that the best estimate of the band splittings, mass parameters, and the crossing points of the bands as a function of strain is obtained by using the experimental volume of zinc-blende GaAs, but the calculated c/a and u parameters. The same approach was used in the previous section discussing the gap changes.

The results for the experimental volume are also shown in Fig. 3. We can see that the conduction-band states are much more sensitive to this change than the valence bands. For the experimental unit-cell volume, Γ_{1c} is lower than Γ_{3c} by 81 meV, but, for the LDA calculated unit-cell volume, Γ_{3c} is lower than Γ_{1c} by 110 meV. This result of a Γ_{1c} CBM at the experimental lattice constant should be more accurate than the result given in the preceding section because we here used an even better converged k-point set, with four divisions along the c axis instead of three. The preceding section was focused on obtaining the WZ-ZB gap difference and, hence, restricted to compatible k-point sets between the ZB and WZ unit cells.

These results indicate that after all we may expect to observe a dipole-allowed transition $\Gamma_{5v} - \Gamma_{1c}$ at zero strain, but our conclusion remains that the conduction band will switch to Γ_{3c} under slight compressive strain before the valence bands cross. Thus, one expects not to see the Γ_{1v}-Γ_{1c} transition in low-temperature luminescence. At any rate, these considerations about polarization dependence would have to be modified by including the spin-orbit coupling.

D. Rashba-Sheka-Pikus Hamiltonian in wurtzite

For further modeling of the nanowires, in the envelope approximation, one needs the band structure parameters of an effective Hamiltonian describing the valence-band

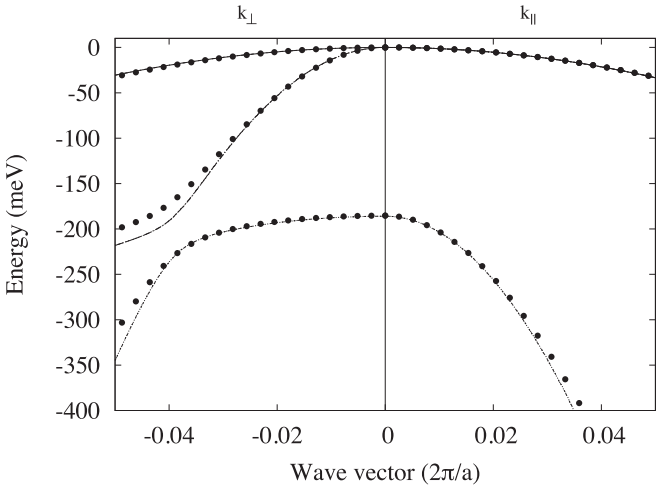

FIG. 4. Band structure of wurtzite GaAs near the valence-band maximum without spin-orbit coupling. The points represent the QSGW results, and the lines represent the RSP fit.

manifold. For wurtzite, we use the Rashba-Sheka-Pikus (RSP) Hamiltonian. The parameters of this model are deduced by fitting to our first-principles band structure results as shown in Figs. 4 and 5 for the QSGW calculation. In the former, the spin-orbit coupling is not included. This allows us to more easily extract the inverse effective mass parameters (A_i, $i = 1,\ldots,7$), and the crystal field splitting Δ_1. In particular, we note that A_7 is related to the avoided band crossing along $k_\perp$ between the crystal field split-off band and the light-hole band. The relations between effective masses and A_i parameters are given in Kim *et al.*[18] The resulting parameters calculated by LDA and QSGW are shown in Table IV. They are all obtained at the experimental lattice volume. The difference of the parameters calculated in Tables IV and V by using instead the LDA equilibrium lattice constant are less than 5%. This can be viewed as the uncertainty of our calculated parameters.

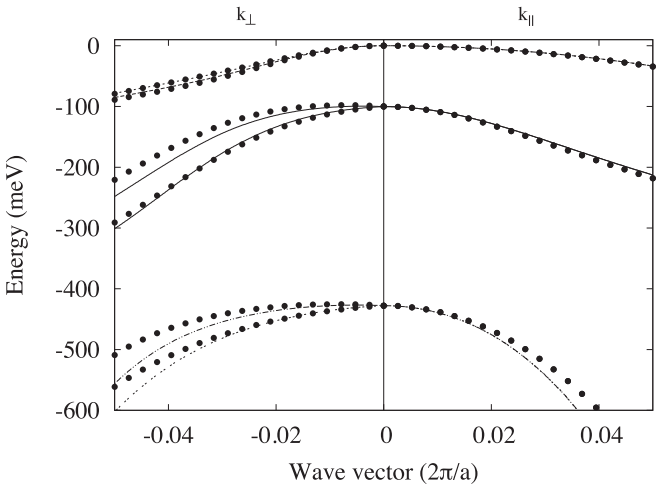

FIG. 5. Band structure of wurtzite GaAs near the valence-band maximum including spin-orbit coupling. The points represent the QSGW including spin-orbit effects results, and the lines represent the RSP fit.

TABLE IV. Effective masses for the conduction- and valence-band edges, excluding spin-orbit effects (in units of free electron mass m_0), and RSP parameters (in units of meV for Δ_i, $\hbar^2/2m_0$ for inverse mass parameters $A_i, i = 1,..,6$, $e^2/2$ for A_7, and eV for D_3, D_4, D_{A_1}) in wurtzite GaAs from the results of LDA calculation, GW calculation with LDA volume [GW (LDA)], and GW calculation with experimental volume [GW (expt.)]

Parameters	LDA	GW (LDA)	GW (expt.)
$m_c^{\parallel}(\Gamma_1)$	0.034	0.060	0.060
$m_c^{\perp}(\Gamma_1)$	0.034	0.082	0.075
$m_c^{\parallel}(\Gamma_3)$	1.096	1.068	1.060
$m_c^{\perp}(\Gamma_3)$	0.091	0.107	0.107
Δ_1	212	186	180
Δ_2	116	116	115
Δ_3	116	114	113
A_1	−29.13	−18.35	−18.39
A_2	−2.39	−1.62	−1.87
A_3	27.87	16.95	17.05
A_4	−13.76	−6.10	−6.26
A_5	14.93	6.44	6.83
A_6	−22.54	−6.22	−7.27
A_7	0.04	0.035	0.035
$m_{hh}^{\parallel}$	0.79	0.72	0.75
$m_{sh}^{\parallel}$	0.03	0.05	0.05
$m_{hh}^{\perp}$	0.82	0.75	0.77
$m_{lh}^{\perp}$	0.03	0.07	0.07
$m_{sh}^{\perp}$	0.42	0.60	0.53
D_3	7.57	7.68	
D_4	−3.79	−3.84	
D_{A_1}	12.7		

Adding the spin-orbit coupling results in two extra parameters Δ_2 and Δ_3 describing the splitting at Γ according to

$$E_{\Gamma_9} = \Delta_1 + \Delta_2,$$
$$E_{\Gamma_{7\pm}} = \frac{\Delta_1 - \Delta_2}{2} \pm \sqrt{\left(\frac{\Delta_1 - \Delta_2}{2}\right)^2 + 2{\Delta_3}^2}. \quad (4)$$

Their effect on the band dispersions is shown in Fig. 5 and the resulting effective masses of the A, B, C valence bands are given in Table V.

E. Conduction-band masses and Kane matrix elements

We also included the conduction-band effective masses in Table IV. From these, we can also deduce the optical matrix

TABLE V. Effective hole masses with spin-orbit effect in unit of electron mass from the results of LDA calculation, GW calculation with LDA volume [GW (LDA)], and GW calculation with experimental volume [GW (expt.)]

Method	$m_A^{\parallel}$	$m_B^{\parallel}$	$m_C^{\parallel}$	$m_A^{\perp}$	$m_B^{\perp}$	$m_C^{\perp}$
LDA	0.79	0.09	0.05	0.06	0.09	0.14
GW (LDA)	0.72	0.12	0.09	0.13	0.19	0.25
GW (expt.)	0.75	0.12	0.09	0.12	0.18	0.23

elements in an eight-band $\mathbf{k}\cdot\mathbf{p}$ approximation. If we neglect spin-orbit coupling, we obtain

$$E_{p\perp} = \frac{2\,|\langle\Gamma_{1c}|\hat{p}_x|\Gamma_{5v}\rangle|^2}{m_0} = \left(\frac{m_0}{m_c^{\perp}} - 1\right)\left(E_{\Gamma_{1c}} - E_{\Gamma_{5v}}\right), \quad (5)$$

$$E_{p\parallel} = \frac{2\,|\langle\Gamma_{1c}|\hat{p}_z|\Gamma_{1v}\rangle|^2}{m_0} = \left(\frac{m_0}{m_c^{\parallel}} - 1\right)\left(E_{\Gamma_{1c}} - E_{\Gamma_{1v}}\right), \quad (6)$$

where $\hat{p}_x$ and $\hat{p}_z$ are momentum operators along x and z directions, respectively. It is well known that the LDA calculation underestimates the band-gap value, but QSGW gives the value that is very close to the experimental value. Therefore, we used $E_{\Gamma_{1c}} - E_{\Gamma_{5v}}$ and $E_{\Gamma_{1c}} - E_{\Gamma_{1v}}$ from QSGW results, which are 1.684 and 1.845 eV, respectively. The values of $E_{p\perp}$ and $E_{p\parallel}$ from our estimation are 18.8 and 28.9 eV, respectively, which are strongly anisotropic.

As we can see in Table IV, the effective mass tensor of the Γ_{1c} state is nearly isotropic, but the effective mass tensor of the Γ_{3c} state is quite anisotropic and quite different from the Γ_{1c} mass tensor. This should facilitate us to recognize whether the CBM is Γ_{3c}- or Γ_{1c}-like in experiment.

F. Strain deformation potentials

As noted earlier, the strain is an important variable in the nanowires. The uniaxial strain effect on the valence-band splitting is described by the equations

$$E_{\Gamma_{5v}} - E_{\Gamma_{1v}} = \Delta_1 + \tfrac{3}{2}D_3\epsilon_{zz} \quad (7)$$

defining the strain deformation potentials D_3 and D_4, where $D_3 = -2D_4$ within the cubic approximation. The optical deformation potential D_{A_1} is defined by

$$E_{\Gamma_{5v}} - E_{\Gamma_{1v}} = D_{A_1} d\ln u\ . \quad (8)$$

These parameters are also included in Table IV. The Γ_{3c} and Γ_{1c} gaps as function of strain can be described by

$$E_{\Gamma_{3c}} - E_{\Gamma_{1c}} = \mu\epsilon_{zz} + \beta \quad (9)$$

with slope parameters $\mu = 19.1$ eV for LDA and $\mu = 21.0$ for QSGW. We also calculated the volume strain effect on the crystal field splitting, the band gap, and the difference between Γ_{3c} and Γ_{1c} levels, which are described by

$$E_{\Gamma_{5v}} - E_{\Gamma_{1v}} = \Delta_1 + D_v\frac{dV}{V}, \quad (10)$$

TABLE VI. Kohn-Luttinger (KL) parameters in units of $\hbar^2/2m_0$.

Method	A	B	C
LDA	−36.2	−3.0	−38.0
GW	−15.6	−3.2	−18.0
Expt.[a]	−15.3	−2.7	−17.4

[a]From Ref. 25.

TABLE VII. Inverse effective mass parameters A_i, $i = 1,\ldots,6$, in units of $\hbar^2/2m_0$ calculated from quasicubic approximation.

Method	A_1	A_2	A_3	A_4	A_5	A_6
LDA	−39.5	−1.4	38.0	−19.0	18.2	−24.6
GW	−19.3	−1.4	18.0	−9.0	8.1	−10.1
Expt.	−18.5	−1.1	17.4	−8.7	7.9	−10.0

$$E_{\Gamma_{1c}} - E_{\Gamma_{5v}} = E^0_{\rm gap} + D_g\frac{dV}{V}, \quad (11)$$

$$E_{\Gamma_{3c}} - E_{\Gamma_{1c}} = E^0_c + D_c\frac{dV}{V}, \quad (12)$$

with $D_v = -227$ meV, $D_g = -7.60$ eV, $D_c = 5.69$ eV, $E^0_{\rm gap} = 460$ meV, and $E^0_c = -110$ meV for the LDA calculation. Our hydrostatic gap deformation potential D_g agrees well with Cardona and Christensen's LDA value for ZB GaAs (Ref. 22) of −7.16 eV. We here do not include absolute deformation potentials of individual band states but only of energy differences because the former require a band lineup calculation between compressed and uncompressed parts of the crystal.[23] Our $D_g = D_1 + D_2$ in Pikus-Bir notation for wurtzite. Relations between the deformation potentials in ZB and WZ and among the WZ ones within the quasicubic approximation can be found in Pikus and Bir.[17]

G. Kohn-Luttinger Hamiltonian in zinc blende

Finally, it is of interest to compare the wurtzite parameters with those of zinc-blende GaAs. For zinc-blende GaAs, the appropriate Hamiltonian is the Kohn-Luttinger (KL) Hamiltonian[24] with parameters A,B,C. These parameters from our calculations and from the experimental values[25] are shown in Table VI. The values obtained from the QSGW calculation agree with the experimental values very well, but the A and C parameters from the LDA calculation are about two times more negative than the experimental values.

In the quasicubic approximation [see Eq. (5) in Ref. 18], the A_i RSP parameters can be related to the KL parameters. The resulting A_i parameters for wurtzite GaAs are shown in Table VII. The values from QSGW and from the experiment are consistent with the wurtzite parameters from the QSGW calculation. However, the parameters from the LDA calculation deviate significantly from the other methods and also from the wurtzite parameters from LDA itself. This indicates that the parameters from the LDA calculation are not reliable for GaAs. This is related to the very strong underestimate of the band gap in GaAs. The conduction-band mass is also very much underestimated by LDA, but our GW value of $0.069m_0$ is in good agreement with the experimental value $0.067m_0$.[20] Very often, people prefer to use the γ_i paramters $\gamma_1 = -\frac{1}{3}(A + 2B)$, $\gamma_2 = -\frac{1}{6}(A - B)$, and $\gamma_3 = -\frac{1}{6}C$ for which we obtain $\gamma_1 = 7.3$, $\gamma_2 = 2.1$, $\gamma_3 = 3.0$ in units of $\hbar^2/2m_0$.

IV. DISCUSSION

Here, we compare our results with previous studies of wurtzite GaAs. Zanolli and von Barth[26] presented LDA Linearized Augmented Plane Wave (LAPW) calculations and later Zanolli *et al.*[6] presented a model GW calculation for the

wurtzite GaAs.[6] They find an increase in gap from zinc blende to wurtzite by 0.047 eV in LDA and by 0.218 eV in GW. We find a smaller gap increase of only 0.080 eV from ZB to WZ almost independent of lattice constant, but quite sensitive on the k-point convergence of the GW self-energy, if we are sure to consider the gap between the same states. The crossings between Γ_{1c} and Γ_{3c}, however, can confuse the issue when only considering the minimum gap.

Recently, De and Pryor[5] presented calculations of various wurtzite semiconductors, including GaAs using semiempirical pseudopotential calculations. They also obtained the $\Gamma_{8c} < \Gamma_{7c}$ in the double-group notation, including spin-orbit coupling. So, this is equivalent to $\Gamma_{3c} < \Gamma_{1c}$. However, their calculation assumed an ideal c/a ratio. Since the actual c/a is larger, it means that their calculation already corresponds to a compressive strain along the c axis. They find a gap reduction from ZB to WZ by only 16 meV, but this is related to their CBM being Γ_{3c} and the uncertainties in structure.

Heiss *et al.*[4] mainly focused on nanowire band structures, including a hybrid functional calculation of WZ an ZB GaAs using the Heyd-Scuseria-Ernzerhof (HSE) functional.[27] They obtain also a gap reduction and obtain a somewhat smaller crystal field splitting. They discuss the effective masses only in the c direction $\Gamma - Z$. They do not discuss the symmetry of the lowest conduction band being Γ_{3c} or Γ_{1c}. But, from their conduction band masses (1.092 for $m_{\parallel}$ for the lowest conduction band close to our 1.096 for the Γ_{3c} and 0.058 for the next band, close to our 0.060 for the Γ_{1c}), it is clear that their CBM has Γ_{3c} symmetry. They report a lower band gap for WZ than for ZB in their table, but this is the $\Gamma_{5v} - \Gamma_{3c}$ gap. From their band structure figure, we can estimate that their $\Gamma_{5v} - \Gamma_{1c}$ gap would in fact be increased compared to the ZB gap in agreement with our calculation.

Experimental data on bulk wurtzite are not available and, thus, any information on the band structure of wurtzite GaAs at present must be extracted indirectly from the nanowire states. However, in nanowires, additional effects control the polarization dependence. For light incident on the nanowire, with wave vector perpendicular to the nanowire, the electric field for polarization parallel to the wire is the same inside and outside the wire, while for polarization perpendicular to the wire (c axis), the electric field is suppressed,

$$E_{\perp}^{\text{in}} = E_{\perp}^{\text{out}} \frac{2\epsilon_2}{\epsilon_1 + \epsilon_2}, \tag{13}$$

where ϵ_1 is the dielectric constant in the wire and ϵ_2 in the medium outside the wire. This tends to favor polarization along the nanowire axis. Furthermore, the confined exciton states in the nanowire no longer have pure light-hole or heavy-hole character and this complicates the ratio of the luminescence for the two polarizations even in zinc blende.[28] It leads, in fact, to the lowest exciton to have polarization along the nanowire axis in zinc blende. For wurtzite, if the crystal field splitting is sufficiently large compared to the quantization energies, the heavy-hole band could, to first approximation, be quantized independently and then leads to a lowest exciton being polarized perpendicular to the wire. At increasing temperature, the transition may then become dominated by parallel polarization again as the next quantized state involving light holes mixed with heavy holes comes into play. Clearly, whether such polarization effects are observed or not will sensitively depend on the crystal field splitting and nanowire radius and, hence, on any residual strain in the nanowire.

Our paper predicts additional interesting effects in suppressing luminescence if the strain reaches the situation where the Γ_{3c} state becomes the conduction band. In mixed wurtzite zinc-blende nanowires, one observes luminescence primarily from the interfaces between the two because the conduction band is lower in the ZB sections, which act as quantum wells within the nanowire.[3] The band alignment in fact is of type II. Thus, we have at the moment no direct information on the character of the conduction-band minimum in pure wurtzite nanowires. A full discussion of the optical properties of such nanowires is outside the scope of this paper, which focuses only on establishing the relevant wurtzite band structure parameters for future studies within the envelope function approximation.

V. CONCLUSIONS

In summary, we have determined the Rashba-Sheka-Pikus effective valence-band Hamiltonian for wurtzite GaAs by fitting to first-principles calculations. We find that the quasicubic approximation from QSGW calculation is very good for GaAs by comparison to the ZB parameters. The uniaxial strain effects on the band structure were examined and show two band crossings (in the valence and conduction bands), which will have important consequences for optical properties. The Kane matrix elements within an eight-band model are shown to be strongly anisotropic. All this indicates the strong anisotropy of wurtzite GaAs and a significant strain dependence. We found that the $\Gamma_{5v} - \Gamma_{1c}$ gap in wurtzite is slightly larger by about 80 meV. The uncertainty in even the sign of this band-gap difference in the previous literature is here avoided by a careful treatment with equivalent k points and analysis of the nature of the conduction band and lattice constant variations.

ACKNOWLEDGMENTS

We thank M. van Schilfgaarde for providing the QSGW and lmf codes and Al. I. Efros for useful discussions on GaAs nanowires. This work made use of the High Performance Computing Resource in the Core Facility for Advanced Research Computing at Case Western Reserve University.

[1] K. Pemasiri, M. Montazeri, R. Gass, L. M. Smith, H. E. Jackson, J. Yarrison-Rice, S. Paiman, Q. Gao, H. Hoe Tan, C. Jagadish, X. Zhang, and J. Zou, Nano Lett. **9**, 648 (2009).

[2] I. Zardo, S. Conesa-Boj, F. Peiro, J. R. Morante, J. Arbiol, E. Uccelli, G. Abstreiter, and A. Fontcuberta i Morral, Phys. Rev. B **80**, 245324 (2009).

[3]D. Spirkoska, J. Arbiol, A. Gustafsson, S. Conesa-Boj, F. Glas, I. Zardo, M. Heigoldt, M. H. Gass, A. L. Bleloch, S. Estrade, M. Kaniber, J. Rossler, F. Peiro, J. R. Morante, G. Abstreiter, L. Samuelson, and A. Fontcuberta i Morral, Phys. Rev. B **80**, 245325 (2009).

[4]M. Heiss, S. Conesa-Boj, J. Ren, H.-H. Tseng, A. Gali, A. Rudolph, E. Uccelli, F. Peiró, J. R. Morante, D. Schuh, E. Reiger, E. Kaxiras, J. Arbiol, and A. Fontcuberta i Morral, Phys. Rev. B **83**, 045303 (2011).

[5]A. De and C. E. Pryor, Phys. Rev. B **81**, 155210 (2010).

[6]Z. Zanolli, F. Fuchs, J. Furthmüller, U. von Barth, and F. Bechstedt, Phys. Rev. B **75**, 245121 (2007).

[7]M. Methfessel, M. van Schilfgaarde, and R. A. Casali, in *Electronic Structure and Physical Properties of Solids. The Use of the LMTO Method*, Lecture Notes in Physics, edited by H. Dreyssé (Springer, Berlin, 2000), Vol. 535, p. 114.

[8]P. Hohenberg and W. Kohn, Phys. Rev. **136**, B864 (1964).

[9]W. Kohn and L. J. Sham, Phys. Rev. **140**, A1133 (1965).

[10]U. von Barth and L. Hedin, J. Phys. C: Solid State Phys. **5**, 1629 (1972).

[11]M. van Schilfgaarde, T. Kotani, and S. Faleev, Phys. Rev. Lett. **96**, 226402 (2006).

[12]M. van Schilfgaarde, T. Kotani, and S. V. Faleev, Phys. Rev. B **74**, 245125 (2006).

[13]T. Kotani, M. van Schilfgaarde, and S. V. Faleev, Phys. Rev. B **76**, 165106 (2007).

[14]L. Hedin and S. Lundqvist, in *Solid State Physics, Advanced in Research and Applications*, edited by F. Seitz, D. Turnbull, and H. Ehrenreich (Academic, New York, 1969), Vol. 23, pp. 1–181.

[15]D. Singh, Phys. Rev. B **43**, 6388 (1991).

[16]T. Kotani and M. van Schilfgaarde, Phys. Rev. B **81**, 125117 (2010).

[17]G. Bir and G. Pikus, *Symmetry and Strain Induced Effects in Semiconductors* (Wiley, New York, 1974).

[18]K. Kim, W. R. L. Lambrecht, B. Segall, and M. van Schilfgaarde, Phys. Rev. B **56**, 7363 (1997).

[19]K. Kim, W. R. L. Lambrecht, and B. Segall, Phys. Rev. B **53**, 16310 (1996).

[20]O. Madelung, M. Schilz, and L.-B. H. Weiss, *Semiconductors, Physics Group IV Elements and III-V Compounds* (Springer, New York, 1982).

[21]P. Grivickas, M. D. McCluskey, and Y. M. Gupta, Phys. Rev. B **80**, 073201 (2009).

[22]M. Cardona and N. E. Christensen, Phys. Rev. B **35**, 6182 (1987).

[23]C. G. Van de Walle and R. M. Martin, Phys. Rev. Lett. **62**, 2028 (1989).

[24]J. M. Luttinger, Phys. Rev. **102**, 1030 (1956).

[25]D. Bimberg, *Advances in Solid State Physics*, edited by J. Treusch (Vieweg, Braunschweig, 1977), Vol. 17, p. 195.

[26]Z. Zanolli and U. von Barth, e-print arXiv:cond-mat/0610066.

[27]J. Heyd, G. E. Scuseria, and M. Ernzerhof, J. Chem. Phys. **124**, 219906 (2006).

[28]A. L. Efros (private communication).